Rotational Tunnelling in Methyl Metal Compounds $X_2(CH_3)_4$ with X = As, Sb, Bi

A. Kuhnen, W. Müller-Warmuth, M. Prager[a], O. Mundt[b], M. Reti[b], and G. Becker[b]

Institut für Physikalische Chemie der Westfälischen Wilhelms-Universität, Schlossplatz 4/7, D-48149 Münster

[a] Institut für Festkörperforschung des Forschungszentrums Jülich, D-52425 Jülich

[b] Institut für Anorganische Chemie der Universität Stuttgart, Pfaffenwaldring 55, D-70550 Stuttgart

Z. Naturforsch. **52a**, 306–316 (1997); received January 21, 1997

Rotational excitations of methyl groups attached to metal atoms of the fifth main group have been investigated in $X_2(CH_3)_4$ crystals with X = As, Sb, Bi by ^1H nuclear magnetic resonance (NMR) relaxation measurements and inelastic neutron scattering (INS). CH_3 rotation has been found to be rather weakly hindered (activation energies between 1.7 kJ/mol and 5.8 kJ/mol) so that quantum effects are important to describe the results. Tunnel splittings between 0.1 μeV and 23 μeV have been observed. Non-equivalent methyl groups in tetramethyldistibane and tetramethyldibismuthane have been identified by both INS and NMR. A consistent description of the T_1 data is possible by Haupt's equation. The rotational potentials could be derived and relations to the crystal structure have been discussed.

1. Introduction

Methyl groups attached to metal atoms of the fourth main group have proved to reorient rather rapidly about their C_3 axes, even in the solid state [1]. Nuclear magnetic resonance (NMR) and inelastic neutron scattering (INS) studies of the tetramethyl compounds of silicon, germanium, tin and lead showed that the potential barriers hindering CH_3 rotation are between 7 and 1 kJ/mol. Four such low barriers quantum effects have to be taken into account to describe the motion and experiments are greatly affected by the splitting of the torsional groundstate ("tunnel splitting"). Both aforementioned techniques provide then more information on the CH_3 rotor and the potential barriers in the molecular crystal than for purely classical regimes. On the other hand, such systems are simple examples of a one-dimensional motion that can be examined between the limits of rotational tunnelling at low temperatures and classical reorientation at high temperature.

Subject of the present paper are molecules in which methyl groups are attached to metals of the fifth main group. Rotational tunnelling in the solid phase was expected to occur as well and a combined INS-NMR study was thought to result in a maximum of information. We hoped to be able to describe the CH_3 rotor with its surroundings rather completely and to find relations to the structure.

Rotational tunnelling of simple molecules is usually well described within the model of single particle rotation. In this model the surrounding is globally represented by a static potential [2]. This potential is usually parametrized as

$$V(\varphi) = \frac{V_3}{2}[1 + (-1)^k \cos 3\varphi] + \frac{V_6}{2}[1 + (-1)^k \cos 6\varphi], \quad (1)$$

and the eigenvalues of the Schrödinger equation for one-dimensional rotation

$$-B\frac{d^2\psi}{d\varphi^2} + [V(\varphi) - E]\psi = 0 \quad (2)$$

are available in numerical form, for phase factors $k = -1, +1$. The rotational constant of the methyl group amounts to $B = 0.6476$ meV $= 0.0625$ kJ/mol ($B/\hbar = 9.84 \cdot 10^{11}$ s^{-1}).

The single particle model was very successful, and data on CH_3 tunnelling are now available for a large number of compounds [2]. In a few cases, however, experimental observations were in disagreement with the model. This motivated the development of more complex models including effects of coupling: coupled pairs of rotors, coupled clusters, coupled chains and the coupling of tunnelling rotation with the centre of

Reprint requests to Prof. W. Müller-Warmuth, Fax: 02 51-83 2 34 41.

0932-0784 / 97 / 0400-0306 $ 06.00 © – Verlag der Zeitschrift für Naturforschung, D-72072 Tübingen

mass motion of the rotor itself [3]. As far as NMR relaxation is concerned, the equation of Haupt has been rather successful to describe the frequency and temperature dependences of T_1^{-1}, even in the presence of nonequivalent CH_3 groups. The behaviour near level crossing, if the NMR frequency approaches the tunnelling frequency, could be reproduced as well, however, as usual apart from the sharp resonance peak which appears to be less pronounced in the experiment.

2. Experimental Procedures

2.1 Sample Preparation and Characterization

The binuclear tetramethyl compounds $(H_3C)_4X_2$ of the heavier group 15 elements arsenic [4, 5], antimony [6–8] and bismuth [6, 9] are liquid at room temperature. Due to their high sensitivity to oxygen and air, respectively, they have to be prepared and handled under an atmosphere of argon using vacuum line techniques and have to be stored in sealed ampoules. Whereas the diarsane and distibane can be purified by vacuum distillation, tetramethyldibismuthane is thermally very labile and decomposes at + 25 °C with nearly quantitative formation of trimethylbismuthane and a black residue of bismuth [9]. Similar to the analogous diphosphane, tetramethyldiarsane is extremely toxic and exhibits a malodorous smell.

Starting materials for the preparation of tetramethyldiarsane and -distibane are the easily accessible halodimethyl derivatives. According to procedures given by Phillips and Vis [5] or Breunig, Breunig-Lyriti, and Knobloch [8], iododimethylarsane and bromodimethylstibane were reduced with lithium or magnesium in diethylether or tetrahydrofuran solution, respectively, to form the products in 80 to 85% yields.

$$2\,Y-X(CH_3)_2 \xrightarrow[-\,2\,MY]{+\,2\,M} X_2(CH_3)_4\,,$$

X = As: Y = I, M = Li;
X = Sb: Y = Br, M = Mg/2.

Tetramethyldibismuthane has been obtained in a 70% yield following the method of Ashe III, Ludwig and Oleksyszyn [10]. At − 60 °C small pieces of sodium, carefully freed from incrustations were added to a stoichiometric amount of trimethylbismuthane in liquid ammonia. After addition of 1,2-dichloroethane to the red solution and a subsequent evaporation of the solvent, the dark crude product was extracted with small portions of *n*-pentane, from which the dibismuthane precipitated at − 30 °C in blue-violet needles.

$$2\,Bi(CH_3)_3 \xrightarrow[-\,2\,Na-CH_3]{+\,4\,Na} 2\,Na-Bi(CH_3)_2$$

$$\cdot \xrightarrow[-\,2\,NaCl;\;-\,C_2H_4]{+\,Cl-C_2H_4-Cl} Bi_2(CH_3)_4\,.$$

Prior to further measurements, the purity of all tetramethyl derivatives was checked by ^1H and ^{13}C NMR spectroscopy of benzene-d_6 or toluene-d_8 solutions (Table 1).

Whereas tetramethyldiphosphane and -diarsane are colourless in the solid as well as in the liquid state, melting or dissolving tetramethyldistibane and -dibismuthane in organic solvents is associated with dramatic colour changes from deep red to pale yellow or from iridescent blue-violet to red, respectively. This unexpected phenomena called thermochromism by several authors [14], have increased the interest in the solid state structures of these relatively low melting compounds considerably:

Isotypic tetramethyldiphosphane and -diarsane crystallize in the monoclinic space group C2/*m* with only a quarter of a molecule in the asymmetric unit of the cell [11]. The molecules of crystallographically imposed symmetry 2/*m* adopt an antiperiplanar conformation (Fig. 1); they are aligned in extended linear chains with relatively long X···X distances. Deep red tetramethyldistibane, however, crystallizes in the orthorombic space group Pnma [12, 15]. The symmetry of the still antiperiplanar molecules is reduced to *m* (Fig. 1) so that now two crystallographic independent $Sb-CH_3$ groups form the asymmetric unit – a finding which is in best agreement with results discussed later

Table 1. Physical constants and NMR data (ppm) of the binuclear compound $X_2(CH_3)_4$. Solvents: benzene-d_6 (X = As, Sb) or toluene-d_8 (X = Bi).

	X = As	X = Sb	X = Bi
mp.	−3 °C [11]	16 °C [12]	−12.5 °C [10]
bp.	155 °C [5]	39 °C/0.01 mbar [8]	[a]
δ^1H	0.96 [13]	0.87 [7]	1.62 [9, 10]
$\delta^{13}C$	6.2 [13]	−10.8 [12]	−18.9 [9, 10]

[a] decomposition at 25 °C [9].

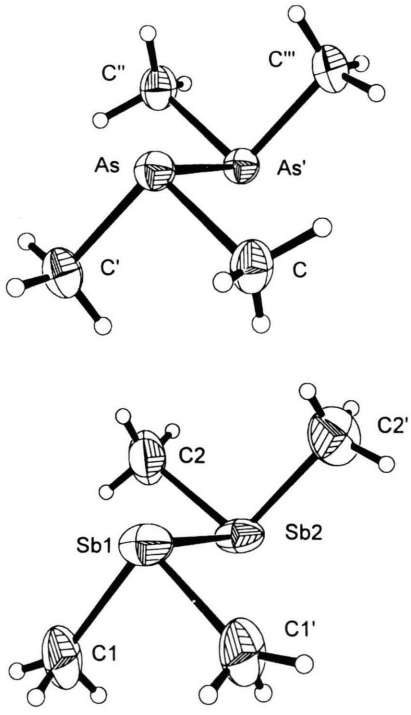

Fig. 1. Molecular structures of tetramethyldiarsane (2/*m*) and – distibane (*m*).

Table 2. Structural data of the binuclear compounds $X_2(CH_3)_4$.

X	P [11]	As [11]	Sb [12]	Bi[a] [16]
Space group	C2/m	C2/m	Pnma	Pnma
X—X (intramolecular; pm)	221.2(1)	242.9(1)	283.8(1)	311
X···X (intermolecular; pm)	381.3(1)	369.9(1)	367.8(1)	359
X—C (pm)	183.8	196.5	213.4/219.0	225[b]
X—X—C (°)	98.3	96.2	94.6/94.3	92[b]
C—X—C (°)	98.8	96.7	92.5/96.0	105[b, c]

[a] Preliminary results; data collection at −150 °C with MoK_α-radiation; single crystal grown from the melt at −19 °C; [b] average of individual values differing by physically meaningless amounts; [c] extremely high value, presumably not correct.

on. Again, the molecules are aligned in extended linear chains of antimony atoms but now X···X contact and X—X bond (X = Sb) approximating each other much more than before (Table 2).

Unfortunately, up to now the structure of iridescent blue-violet tetramethyldibismuthane is not known with the same accuracy as those of the lighter homologues. According to refinements based on data sets collected at various temperatures and wavelengths, the compound most probably crystallizes isotypically to the antimony derivative [16]. With these results taken to be correct, molecules of antiperiplanar conformation are aligned in chains with relatively short intermolecular Bi···Bi contacts. The carbon positions, however, could not be refined satisfactorily due to severe disorder – presumably twinning – problems combined with a strong absorption. As a consequence, crystal and molecular symmetry of tetramethyldibismuthane remain uncertain to some degree and the presence of two topologically distinct methyl groups in a 1:2 ratio as reported below cannot be substantiated from a structurel point of view.

2.2 Inelastic Neutron Scattering

In the single particle model, the neutron scattering function of a methyl group is at low temperature [17]

$$S(Q,\omega) = \left(\frac{5}{3} + \frac{4}{3} j_0(Qd)\right)\delta(\omega) + \left(\frac{2}{3} - \frac{2}{3} j_0(Qd)\right) \cdot \{\delta(\omega+\omega_t) + \delta(\omega-\omega_t)\}\,. \quad (3)$$

It contains one elastic and two inelastic lines, the latter with energy loss or gain at the tunnelling frequency ω_t. The inelastic structure factors, i.e. the dependence of the intensity of the tunnelling line on momentum transfer Q, reflect the geometry of the rotor via the proton-proton distance d. For a single methyl group the ratio between inelastic and elastic intensity is

$$r = \frac{I^1_{\text{inel}}}{I^1_{\text{el}}} = \frac{\frac{2}{3} - \frac{2}{3} j_0(Qd)}{\frac{5}{3} + \frac{4}{3} j_0(Qd)}\,.$$

This ratio is reduced in the presence of CH_3 groups with unresolved tunnel splitting which contribute to elastic scattering only. If one of n methyl groups shows resolved splitting, then the observed ratio is $r' = r/[n(1+r) - r]$. For more details, see review [18].

In addition to the tunnel splitting (usually in the μeV range) the librational modes in the meV range may yield information on the rotational potential. Identification and assignment of the lines is, however, not always straightforward, especially in the presence of inequivalent methyl groups as in this work.

Various spectrometers were used. Tunnelling spectra of $Bi_2(CH_3)_4$ were measured at the backscattering spectrometer BSS at the research FRJ2/DIDO in

Jülich [19]. An incoming wavelength of $\lambda = 6.28$ Å was selected from the continuous spectrum of neutrons by a mixed SiGe monochromator crystal oriented at backscattering condition. The content of Ge is such that an energy offset of 12 μeV was obtained with respect to the analyzer crystals consisting of pure Si. Using the highest velocity of the Doppler drive moving the monochrometer crystal an energy range $-3 < \hbar\omega/\mu\text{eV} \leq 27$ could be explored.

Tunnelling spectra of $Sb_2(CH_3)_4$ were obtained from the inverse time-of-flight backscattering spectrometer IRIS of the RAL, UK [20]. The spectrometer was used in two configurations, first with a pyrolytic graphite PG 002 analyser and an energy resolution of 15 μeV, later with the MICA 004 analyser ($\lambda_f = 9.6$ Å) and an energy resolution of 4 μeV. The same spectrometer was employed to study $As_2(CH_3)_4$, where, however, no inelastic effect was found.

Excitations in the meV range were studied using the thermal time-of-flight spectrometer SV 22 in Jülich [19]. With an incoming energy of 36 meV energy transfer up to 30 meV can be identified. In this energy range the scattering function weights the intensities with the product of the scattering cross section of the moving atoms and the mean-square displacement [21]. Both factors favour the observation of CH_3 librational modes. The corresponding peaks should broaden and weaken significantly with increasing temperatures. This behaviour supports the assignment to librational modes of the methyl groups.

2.3 NMR-T_1 Measurements

The procedures of obtaining information on CH_3 tunnelling from ^{1}H-NMR, and especially from measurements of the spin-lattice relaxation time T_1, were discussed in various previous papers [22]. T_1 was measured by $90°-\tau-90°$ pulse sequences at two different frequencies (15 MHz and 30 MHz) and at temperatures between about 10 K and 100 K. For many temperatures the relaxation was non-exponential as a consequence of the symmetry-restricted spin diffusion [23], and therefore only the initial slope of the plot $\ln\{(M_0 - M_z)/M_0\}$ versus time had to be evaluated (the components M_0 and M_z of the proton magnetization have the usual meaning). The accuracy of the $^1/T_1$ data suffers of course from the non-exponentiality and is only of the order of 10%. Near the level-crossing of $As_2(CH_3)_4$ it is worse.

The experimental T_1^{-1} vs. $10^3/T$ curves were fitted by the equation

$$1/T_1 = C_1 \sum_{n=-2}^{+2} \frac{n^2 \tau_c}{1+(\omega_t + n\omega_0)^2 \tau_c^2} + C_2 \sum_{n=1}^{2} \frac{n^2 \tau_c}{1+n^2 \omega_0^2 \tau_c^2} \tag{4}$$

first proposed by Haupt [24]. In (4), C_1 accounts for dipole-dipole interactions that are connected with a change in the symmetry of the CH_3 rotor from A to E and C_2 for transitions without symmetry change, which are forbidden if only intra-methyl couplings are relevant. The temperature dependence of the correlation time τ_c was approximated by

$$\tau_c^{-1} = (\tau_0')^{-1} \exp(-E_A'/RT) + (\tau_0'')^{-1} \exp(-E_A''/RT), \tag{5}$$

as verified in previous papers. The limiting high-temperature value E_A' may be identified with the (classical) activation energy E_A for CH_3 reorientation in the hindering potential. For low barriers the low-temperature limiting value E_A'' was often found to approach E_{01}, the energy separation between the torsional ground and first excited states [25].

To describe such relaxation data properly it proved to be necessary to have regard to the temperature depencence of the tunnelling frequency. To account for the rapid decrease with temperature, and considering the available experimental data mostly obtained from neutron scattering, we used the empirical relation [22].

$$\omega_t(T) = \frac{\omega_t^0}{1 + aT^6}. \tag{6}$$

The coefficient a is characteristic of the respective material and is of the order of magnitude of $10^{-10}\,\text{K}^{-6}$.

3. Results

$As_2(CH_3)_4$

Figure 2 shows the ^{1}H-NMR spin-lattice relaxation rates plotted against reciprocal temperatures. The right hand part of the dependences looks extremely anomalous, especially the strong frequency dependence at low temperature. Near 30 K the relaxation is greatly non-exponential, especially that at $\omega_0/2\pi = 15$ MHz. There occurs a level-crossing peak when the tunnelling frequency matches the applied frequency, $\omega_t = \omega_0$. At still lower temperature the condition $\omega_t = 2\omega_0$ is not yet reached, but the resonance term

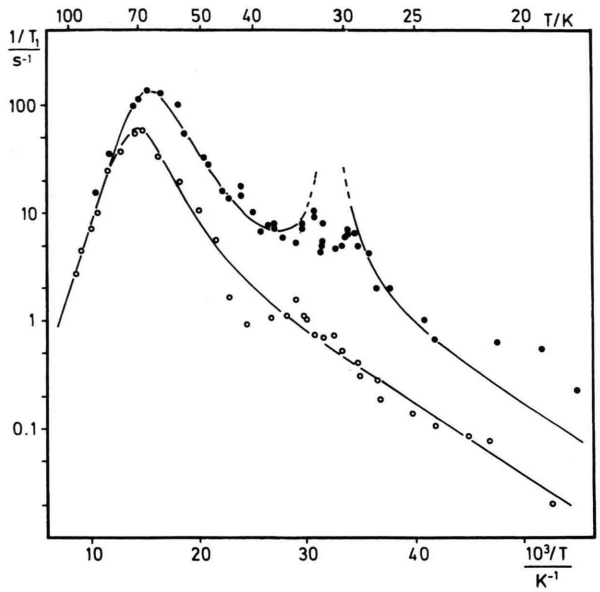

Fig. 2. Experimental ^1H NMR spin-lattice relaxation rates (points) measured at two different frequencies and various temperatures for $As_2(CH_3)_4$. The data are plotted versus reciprocal temperatures and fitted by the solid lines as explained in the text. Solid symbol 15 MHz, open symbol 30 MHz.

proportional to $[1+(\omega_t-2\omega_0)^2\tau_c^2]^{-1}$ becomes already large so that excessive relaxation takes places. The $\omega_0/2\pi = 30$ MHz curve is less affected because here $2\omega_0, \omega_0 > \omega_t$ holds. The left hand part of Fig. 2 behaves "classically" with the maxima near $\omega_0\tau_c \approx 0.63$ and the correct frequency dependence.

The solid lines in Fig. 2 are an attempt to fit the points by (4)–(6), assuming level-crossing of the 15 MHz curve at 32.4 K. As usual, the experiments do not reflect the peak near 30 K as sharp as represented by (4). In agreement with the crystal structure (Sect. 2.1) the methyl groups are all equivalent. The parameters of the fitting procedure are collected in Table 3.

Neutron scattering experiments at a sample temperature of $T = 5$ K at the IRIS spectrometer did not show inelastic effects between 2 μeV and 655 μeV. This is in agreement with the NMR-T_1 experiments leading to a single tunnel frequency of the order of magnitude of 0.1 μeV. In the meV range, however, a well-structured spectrum was observed with the SV22 spectrometer, cf. Figure 3. The peak at 18.5 meV could be identified as the only methyl librational mode. The weakly pronounced doublet rather than singulet may be explained in terms of either a symmetry-conditioned splitting or dispersion. The latter was observed for example for *p*-xylene [26], and could be confirmed by a lattice dynamical calculation.

$Sb_2(CH_3)_4$

The NMR-T_1 relaxation rates (Fig. 4) reveal two maxima if plotted against reciprocal temperatures where the first one near 44 K is nearly independent of frequency, and the second one near 19 K and 20 K is rather broad. The frequency and temperature dependences are characteristic of tunnelling frequencies $\omega_t \gg \omega_0$. A fit of the points by (4)–(6), using one set of parameters as for $As_2(CH_3)_4$ is, however, not possible. Supported by structure determinations which predict two types of inequivalent methyl groups (Sect. 2.1) and as well suggested by the INS experiments discussed further below, we describe the results by the superposition of two curves of the type of (4). Each

Table 3. Numerical values of tunnel splittings and librational excitations measured by inelastic neutron scattering, and of the parameters derived from the NMR-T_1 measurements; (.)[a]: not directly measured, but estimated from the T_1 fit; (.)[b]: only the sum $2C_1 + C_2$ is accurately determined.

Compound	INS		NMR						
	$\hbar\omega_t^0$ / μeV	E_{01} / kJ/mol	E_A' / kJ/mol	τ_0' / 10^{-13} s	E_A'' / kJ/mol	τ_0'' / 10^{-10} s	C_1 / 10^9 s^{-2}	C_2 / 10^9 s^{-2}	a / 10^{-10} K^{-6}
$As_2(CH_3)_4$	(0.1)[a]	1.79	5.8	1.5	1.7	15	(3.5)[b]	(1.7)[b]	7
$Sb_2(CH_3)_4$ (I)	(1)[a]		3.9	2.0	1.3	2	1.2	0.32	1.9
(II)	23		1.7	4.0	0.34	10	2.0	0.40	2.3
$Bi_2(CH_3)_4$ (I)	3.35		3.0	0.6	0.4	0.9	2.8	$\ll 0.1$	3.9
(II)	13.8 16.7	1.06	2.0	1.0	1.1	0.03	2.4	0.14	11.0

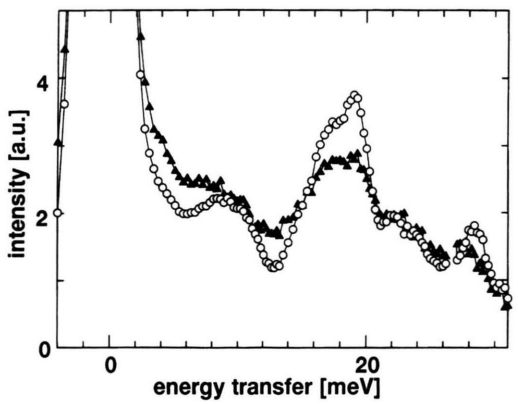

Fig. 3. INS spectrum of $As_2(CH_3)_4$ in the meV regime measured with the time-of-flight spectrometer SV 22, KFA, D-Jülich. Standard programs were used to transform the data to $S(Q, \omega)$. The incident wavelenght was $\lambda = 1.52$ meV. Solid symbol: $T = 5$ K, open symbol: $T = 60$ K.

belongs to one half of the number of tunnelling or reorienting methyl groups in tetramethyldistibane. Type I of the CH_3 groups contributes essentially to the high temperature part of the $1/T_1$ curve of Fig. 4, the much more freely rotating CH_3 groups (II) cause relaxation down to rather low temperatures.

The solid line of Fig. 4 represents this interpretation and the fitting parameters are again listed in Table 3. In the absence of level-crossing peaks (both tunnel splittings are larger than the NMR frequencies) the T_1 experiments can only provide the order of magnitude of the tunnelling frequencies.

The INS spectrum of $Sb_2(CH_3)_4$ is shown in Figure 5. One tunnelling transition is well resolved at an energy transfer $\hbar\omega_t^0 = 23$ μeV at $T = 2$ K. Its intensity amounts to 0.14 in units of the elastic intensity at the average momentum transfer $Q = 1.41$ Å^{-1}. For a single type of methyl groups the ratio r of inelastic to inelastic intensities is calculated to amount to 0.26. The smaller values observed show that a certain part of the CH_3 groups is more strongly hindered and scatters purely elastically. If a second nonequivalent species of equal weight is present, then the new ratio $r' = r/(2 + r)$ corresponds to the experimental result. Thus half of the methyl groups tunnel with a high rate, whereas the second half is more strongly hindered, in agreement with the T_1 data and with the occurrence probabilities derived from the crystal structure [12].

The INS spectrum in the meV range does not show much structure (not shown). Probably, because of the interaction with lattice vibrations, librational modes could not be identified.

$Bi_2(CH_3)_4$

The T_1^{-1} data (cf. Fig. 6) remind of those of tetramethyldistibane, but the maxima appear to be less separated. Again, they cannot be fitted by assuming rotation or tunnelling of equivalent methyl groups.

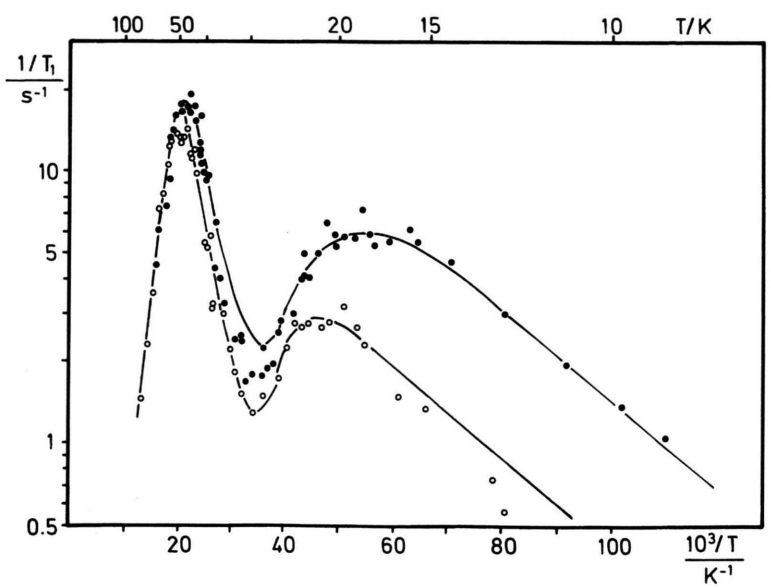

Fig. 4. Same as Fig. 2, but for $Sb_2(CH_3)_4$.

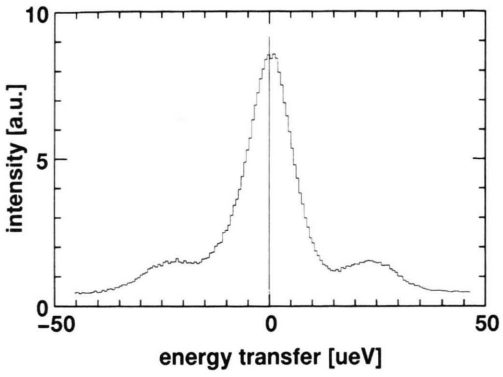

Fig. 5. INS tunnelling spectrum of $Sb_2(CH_3)_4$ measured with the IRIS spectrometer at the RAL, UK-Chilton, with $\lambda = = 6.7$ Å, $Q = 1.7$ Å^{-1} and $T = 2$ K.

Three maxima occur in the representation of Fig. 6, two between 27 K and 40 K nearly independent of frequency and one frequency dependent maximum near 17 K and 19 K, respectively. The behaviour is characteristic of $\omega_t^0 \gg \omega_0$. The crystal structure is not known in detail but there is evidence that it is similar to that of $Sb_2(CH_3)_4$ with inequivalent CH_3 groups. A clear sign of the inequivalency are the INS spectra with three tunnel peaks (see below). Using this result we fitted the points of Fig. 6 by assuming two types of inequivalent methyl groups with tunnel splittings of 3.4 μeV and 15 μeV, respectively, and an intensity ratio of 2:1. Each of them was described by (4) with (5) and (6) for $\tau_c(T)$ and $\omega_t(T)$; the parameters are listed in Table 3.

Figure 7 shows the INS spectrum in the μeV regime where the solid line represents a fit of the elastic and three inelastic lines, each one modelled by a δ-function convoluted with the resolution function. Tunnelling energies extracted from this representation are 3.35 μeV, 13.8 μeV and 16.7 μeV with intensities (in units of the elastic intensity) 0.137, 0.044 and 0.022, respectively. The temperature evolution of the spectrum was measured up to 30 K (not shown). At low temperature the tunnel splittings, especially those of the lines at 14 μeV and 17 μeV, increase before displaying the usual decrease above 20 K. For such temperatures the doublet line at the high energy transfer can no longer be resolved. The small intensity ratios given above seem to indicate that only about one fourth of the tunnel modes are resolved. This is at variance, however, with the NMR results which give an activation energy of about 3 kJ/mol (corresponding to the tunnel splitting of about 4 μeV) for the most hindered process.

In the meV range, with the moderate elastic energy resolution of 2.8 meV, the spectrum shows two peaks near 11 meV and 22 meV (Figure 8). Both peaks broaden and weaken significantly with increasing temperature. Assignment is not at all straightforward, but taking into consideration the NMR results the

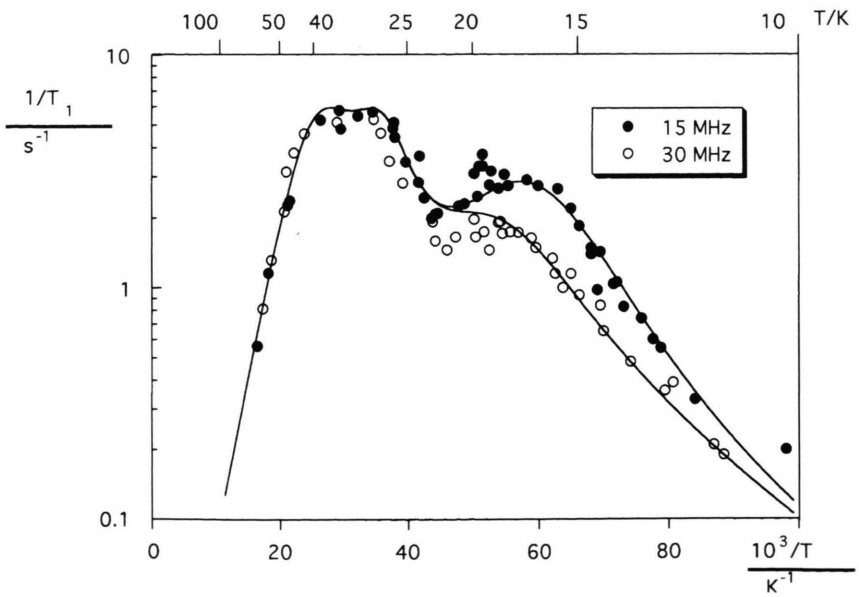

Fig. 6.
Same as Fig. 2,
but for $Bi_2(CH_3)_4$.

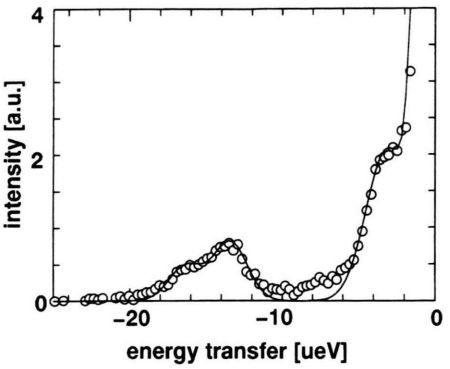

Fig. 7. Tunnelling spectrum of $Bi_2(CH_3)_4$ measured with the BSS spectrometer of the KFA, D-Jülich. $\lambda = 6.28$ Å, $Q = 1.73$ Å^{-1}, $T = 5$ K.

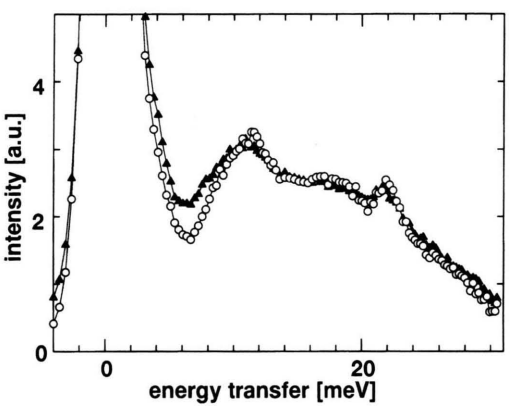

Fig. 8. Same as Fig. 3, but for $Bi_2(CH_3)_4$; $T = 22$ K and 40 K.

11 meV line is assumed to belong to those CH_3 groups which exhibit the high energy tunnel splittings. The excitation for those rotors which have the tunnel splitting near 4 μeV and the activation energy of 3.0 kJ/mol seems to be hidden under the large peak near 13 or 14 meV. The peak at 22 meV could belong to an excited torsional transition or a lattice excitation.

In order to secure that the observed three tunnel splittings belong really to the CH_3 rotation in $Bi_2(CH_3)_4$ and not to that of $Bi(CH_3)_3$ which was used as a primary product in the synthesis, the INS spectra of trimethylbismuthane were also studied. A tunnel splitting of 5.5 μeV was observed which does not coincide with one of the $Bi_2(CH_3)_4$ lines.

4. Discussion

4.1 Individual Results

Among the materials studied in this work, tetramethyldiarsane possesses the highest barrier hindering methyl group rotation. But quantum effects are still important. In agreement with the NMR results, above about 1 μeV no INS tunnelling line could be observed. A direct reference to the occurrence of tunnelling is the (strongly damped) level-crossing peak near 30 K (Fig. 2), indicating a tunnelling frequency of 15 MHz ($\hbar\omega_t = 0.062$ μeV). Extrapolation to very low temperature in combination with the $1/T_1$ – fit leads then to $\omega_t^0/2\pi \approx 24$ MHz ($\hbar\omega_t^0 \approx 0.1$ μeV).

In agreement with the crystal structure (Sect. 2.1) in $As_2(CH_3)_4$, all the CH_3 groups are equivalent. This is supported by the INS experiments in the meV range as well (Figure 3). The spectrum is well structured, and because of the relatively high rotational potential the librational excitation is rather high and interacts little with the phonons. The result is the strong peak and its characteristic behaviour.

Tetramethylbistibane is distinguished by two types of non-equivalent methyl groups of equal weight in the unit cell. This agrees with both the NMR and the INS experiments. The frequency and temperature dependence of T_1^{-1} (Fig. 4) can only be explained in terms of two different methyl rotors, one mainly contributing to the first maximum and the second one mainly to the second maximum. By INS only a single somewhat broadened line was observed and the ratio of inelastic to elastic intensities suggests that one half on the CH_3 groups contribute to this line. The second half appears to be more strongly hindered and escapes observation in this experiment. Different from many other organometallic compounds with non-equivalent methyl groups, in this particular case the difference of the activation energies and tunnel splittings is exceptionally large.

Unfortunately, no librational excitations could be identified in $Sb_2(CH_3)_4$. Like in many previous experiments, the reason may be a rather strong interaction with the lattice modes. There seems to be a correlation to the NMR-T_1 measurements as well. The apparent activation energy from the low temperature slope of the T_1^{-1} versus $1000/T$ plot (Fig. 4) does no longer correspond to E_{01}, the energy separation between the librational ground and first excited states.

The results of tetramethyldibismuthane show several similarities as compared with those of the anti-

mony compound. We find again non-equivalent CH_3 groups, but two or three tunnel splittings could be observed in the INS experiment. From the NMR-T_1 measurements it can be concluded that there is no further excitation with a lower tunnel splitting, but no distinction can be made whether the splittings at 13.8 μeV and 16.7 μeV belong to an equivalent set of CH_3 or not. Only one librational excitation was observed (Fig. 8) which is assigned in combination with the other data to CH_3(II). $E_{01}$for CH_3(I) should lie near 13 meV and is hidden.

The crystal structure of $Bi_2(CH_3)_4$ is believed to be similar to that of $Sb_2(CH_3)_4$ with at least two types of inequivalent methyl groups in the unit cell. According to the results given here, however, the weight is not equal, but 2:1 in favour of CH_3(I). This can be concluded from the INS intensities of the tunnel splittings (the two neighbouring peaks at 13.8 μeV and 16.7 μeV are taken as one belonging to the CH_3(II) types).

4.2 Tunnel Splittings, Rotational Potentials and Structure

The observed tunnel splittings $\hbar\omega_t^0$ (or tunnelling frequencies $\omega_t^0/2\pi$) increase from about 0.1 μeV (24 MHz) to 23 μeV (5.6 GHz) or 16.7 μeV (4.0 GHz) if going from the arsane to the stibane (II) or bismuthane (II) methyl groups (cf. Table 1). A clear correlation to the molecular structure can be stated.

As already observed for the tetramethyl compounds of the metals of the fourth main group [1], the tunnel splittings depend again mainly on the bond length r_{XC} between metal (X) and carbon atom (C). Figure 9 shows a plot of $\hbar\omega_t^0$ against r_{XC} for both classes of compounds. Bond lengths for $X_2(CH_3)_4$ (X = As, Sb) were taken from Table 2, those for $X(CH_3)_4$ (X = Si, Ge, Sn, Pb) were given in [1] with the appropriate references. The used tunnel splittings and r_{XC} values are once more listed in Table 4 of this work or in Tables 2 and 3 of [1]. The exponential dependence of $\hbar\omega_t^0$ on r_{XC} of Fig. 9 corresponds approximately to that already proposed in [1]. The representation of $\hbar\omega_t^0$ solely depending on the X–C distance looks quite satisfactory, in particular if the different molecular structures of the various materials are concerned. Figure 9 suggests an estimate of r_{XC} in $Bi_2(CH_3)_4$, which should be of the order of 210 pm and 220 pm, respectively, for the two non-equivalent CH_3 groups, the latter value is in satisfactory agreement with that indicated in Table 2.

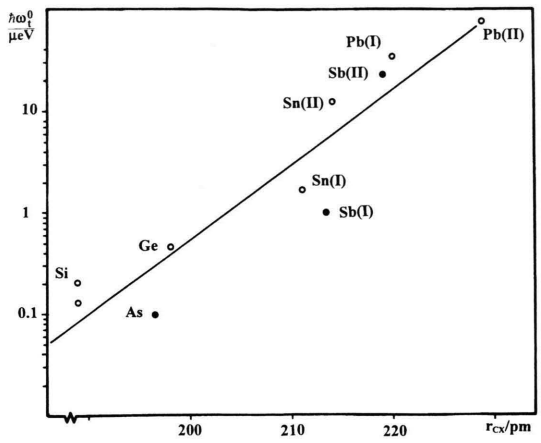

Fig. 9. Tunnel splittings versus the length of the X-C bond for X = Si, As, Ge, Sn, Sb and Pb.

Table 4. Experimental tunnel splittings and derived values for the (threefold) rotational potential and the librational excitation; (.)[a]: identified with experimental data. The last column lists the bond lengths between the metal and (methyl) carbon atoms.

Compound	$\hbar\omega_t^0$ / μeV	V_3 / kJ/mol	E_{01} / kJ/mol	r_{XC} / pm
$As_2(CH_3)_4$	0.1	6.9	(1.79)[a]	196.5
$Sb_2(CH_3)_4$ (I)	1	4.8	1.50	213.4
(II)	23	2.2	0.96	219.0
$Bi_2(CH_3)_4$ (I)	3.35	3.8	1.31	
(II)	15	2.6	(1.06)[a]	

The eigenvalues of the Schrödinger equation (2) with a potential (1) are available in numerical form [27] and can be used to calculate the rotational potentials if $\hbar\omega_t^0$ and the activation energy $E_A \approx E_A'$ are known. Knowledge of the energy separation E_{01} (available for $As_2(CH_3)_4$ and $Bi_2(CH_3)_4$(I), cf. Table 3) may serve as an additional control of the consistency of the procedure. For all the five types of methyl groups of Table 4, within the limits of accuracy, the potential turned out to be purely threefold. The V_3 values as obtained from (2) with (1) with the experimental data are listed in this table. We find a linear dependence of V_3 on the X–C bond length for all the CH_3 groups attached to metal atoms of the fourth and fifth main group of the periodic table. The potential, i.e., the hindrance of the CH_3 rotation appears to be the weaker the larger the metal atom is. This points to steric effects and mutual hindrances of the various

CH_3 groups as the main reasons of the internal barriers. Altogether, the potential is rather low for all these compounds, comparable to those in systems with methyl rotors attached to aromatic and heterocyclic carbon atoms or to carbonyl groups.

4.3 Anomalous Relaxation

The spin-lattice relaxation of the investigated materials deviates greatly from the classical BPP [28] behaviour, since at lower temperature the methyl rotation is greatly determined by quantum effects. For large tunnel splittings, $\omega_t \gg \omega_0$, as for the methyl groups in the antimony and bismuth compounds, the first term of (4) reduces to

$$\frac{1}{T_1} = \frac{10\, C_1}{1 + \omega_t^2\, \tau_c^2}. \tag{7}$$

Then two maxima are observed, one frequency independent maximum at higher temperature near $\omega_t \tau_c \approx 1$, and the other one at $\omega_0 \tau_c \approx 0.63$. Such a behaviour dominates T_1^{-1} in Figs. 4 and 6, although, because of the superposition of two curves due to inequivalent CH_3 groups, the separation of all of the various maxima is not immediately visible at first sight. For $As_2(CH_3)_4$ the tunnelling frequency appears to be of the same order of magnitude as the NMR frequency ω_0, and all the terms of (4) contribute. The resonance terms at $\omega_t = \omega_0, 2\,\omega_0$ are especially important, cf. Figure 2.

Considering the parameters of Table 3, the values of τ_0' (order of magnitude: 10^{-13} s) and E_A' describe the classical reorientation at sufficiently high temperatures. E_A' corresponds to the (classical) activation energy E_A which is the energy separation between barrier height and (librational) groundstate. The values for $As_2(CH_3)_4$, $Sb_2(CH_3)_4$(I) and $Bi_2(CH_3)_4$(I) were immediately taken from the high temperature part of the $T_1^{-1}(T^{-1})$ dependences, those for $Sb_2(CH_3)_4$(II) and $Bi_2(CH_3)_4$(II) are less accurate since they are the result of the superposition.

Tables 3 and 4 show that the apparent low temperature activation energies E_A'' correspond in favourable cases to E_{01} (see also [1], [22], [24–26]). Clear exceptions are $Sb_2(CH_3)_4$(II) and $Bi_2(CH_3)_4$(I), the same systems in which also no proper INS peaks were found in the meV range. τ_0'' values have the usual order of magnitude.

The intramethyl relaxation strength C_1 can be written [13, 14]

$$C_1 = \frac{9}{40}\left(\frac{\mu_0}{4\pi}\right)^2 \frac{\gamma^4 \hbar^2}{b^6}\, p\, \delta^2 (1 + X_1)$$
$$= 4.0 \cdot 10^9\, p\, \delta^2 (1 + X_1)\, s^{-2} \tag{8}$$

with the usual meaning of μ_0, γ and $\hbar$. $b = 178.1$ pm is the proton-proton distance in the CH_3 group. The "relaxation efficiency" factor δ^2 [24] is of the order of magnitude of 1. p denotes the ratio of relaxing methyl protons to the total number of protons. Since we have only CH_3 protons, but sometimes non-equivalent groups, for $As_2(CH_3)_4$ $p = 1$ holds, but for both methyl groups in $Sb_2(CH_3)_4$ $p = 0.5$, and $p = 0.67$ for $Bi_2(CH_3)_4$(I) and $p = 0.33$ for $Bi_2(CH_3)_4$(II). X_1 accounts for the influence of neighbouring methyl groups to excite transitions.

Inspection of Table 3 shows that the C_1 data have the correct order of magnitude with some deviations as usually observed. Depending on the structure, with the exception of $As_2(CH_3)_4$, C_2 is clearly smaller than C_1. This means, though observable, intermethyl relaxation plays a minor role.

Acknowledgements

The authors would like to thank Dr. Leo van Wüllen for his support to describe the NMR-T_1 data numerically by superposition of two contributions, Dr. W. Kagunya and the Rutherford-Appleton Laboratories for the use of the IRIS spectrometer and experimental support, and Dr. M. Pionke for the measurements at the backscattering spectrometer in Jülich.

[1] W. Müller-Warmuth, K. H. Duprée, and M. Prager, Z. Naturforsch. **39a,** 66 (1984).
[2] M. Prager and A. Heidemann, Rotational Tunnelling and Neutron Spectroscopy: A Compilation, ILL Internal Report PR 87 T (1987), and Chem. Rev. (1997), accepted for publication.
[3] M. Havighorst and M. Prager, Physica B **226,** 178 (1996).
[4] L. C. Cadet de Gassicourt. Mem Math Phys. **3,** 623 (1760).
[5] J. R. Phillips and J. H. Vis, Can. J. Chem. **45,** 675 (1967).
[6] F. A. Paneth, Trans. Faraday Soc. **30,** 179 (1934); F. A. Paneth and H. Loleit, J. Chem. Soc **1935,** 366.
[7] H. A. Meinema, H. Martens, and J. G. Noltes, J. Organomet. Chem. **51,** 223 (1973).
[8] H. J. Breunig, V. Breunig-Lyriti, and T. P. Knobloch, Chemiker-Ztg. **101,** 399 (1977).
[9] A. J. Ashe, III and E. G. Ludwig, Jr., Organometallics **1,** 1408 (1982).
[10] A. J. Ashe, III, E. G. Ludwig, Jr., and J. Oleksyszyn, Organometallics **2,** 1859 (1983).
[11] O. Mundt, H. Riffel, G. Becker, and A. Simon, Z. Naturforsch. **43b,** 952 (1988).
[12] O. Mundt, H. Riffel, G. Becker, and A. Simon, Z. Naturforsch. **39b,** 317 (1984).
[13] G. Becker and M. Reti, unpublished measurements.
[14] A. J. Ashe, III, W. Butler, and T. R. Diephouse, J. Amer. Chem. Soc. **103,** 207 (1981); see also: A. J. Ashe III, Acta. Organomet. Chem. **30,** 77 (1990).
[15] A. J. Ashe, III, E. G. Ludwig, Jr., J. Oleksyszyn, and J. C. Huffman, Organometallics **3,** 337 (1984).
[16] J. Baumgarten, Thesis, University of Stuttgart 1988.
[17] W. Press, Single Particle Rotations in Molecular Crystals, Springer Tracts in Modern Physics **92,** Springer, Berlin 1981.
[18] C. J. Carlile and M. Prager, Int. J. Mod. Phys. **B7,** 3113 (1993).
[19] T. Springer, Experimentiereinrichtungen am FRJ 2 der KFA Jülich, to be obtained from the Institut für Neutronenstreuung, IFF, KFA Jülich, D-52425 Jülich.
[20] C. J. Carlile and M. Adams, Physica **B182,** 431 (1992).
[21] J. Howard and T. C. Waddington, in Molecular Spectroscopy with Neutrons, Advances in Infrared and Raman Spectroscopy (R. J. H. Clark and R. E. Hester, eds.), Vol. **7,** Heyden, London 1980.
[22] T. K. Jahnke, W. Müller-Warmuth, and M. Bennati, Solid State NMR **4,** 153 (1995), and references therein.
[23] S. Emid and R. A. Wind, Chem. Phys. Lett. **33,** 269 (1975).
[24] J. Haupt, Z. Naturforsch. **26,** 1578 (1991).
[25] H. Langen, A. S. Montjoie, W. Müller-Warmuth, and H. Stiller, Z. Naturforsch. **42a,** 1266 (1987), and references therein.
[26] M. Prager, R. Hempelmann, H. Langen, and W. Müller-Warmuth, J. Phys.: Condens. Matter **2,** 8625 (1990).
[27] R. F. Gloden, Euratom Reports EUR 4349 and EUR 4358 (1970).
[28] N. Bloembergen, E. M. Purcell and R. V. Pound, Phys. Rev. **73,** 679 (1948).